

# Search for Mono-Higgs Signals at the LHC in the $B - L$ Supersymmetric Standard Model

---

W. Abdallah<sup>1,2</sup>, A. Hammad<sup>1</sup>, S. Khalil<sup>1</sup> and S. Moretti<sup>3</sup>

<sup>1</sup>*Center for Fundamental Physics, Zewail City of Science and Technology, 6 October City, Giza 12588, Egypt.*

<sup>2</sup>*Department of Mathematics, Faculty of Science, Cairo University, Giza 12613, Egypt.*

<sup>3</sup>*School of Physics and Astronomy, University of Southampton, Highfield, Southampton SO17 1BJ, UK.*

*E-mail:* [wabdallah@zewailcity.edu.eg](mailto:wabdallah@zewailcity.edu.eg), [ahammad@zewailcity.edu.eg](mailto:ahammad@zewailcity.edu.eg),  
[skhalil@zewailcity.edu.eg](mailto:skhalil@zewailcity.edu.eg), [s.moretti@soton.ac.uk](mailto:s.moretti@soton.ac.uk)

**ABSTRACT:** We study mono-Higgs signatures emerging in the  $B - L$  supersymmetric standard model induced by new channels not present in the minimal supersymmetric standard model, i.e., via topologies in which the mediator is either a heavy  $Z'$ , with mass of  $\mathcal{O}(2 \text{ TeV})$ , or an intermediate  $h'$  (the lightest CP-even Higgs state of  $B - L$  origin), with mass of  $\mathcal{O}(0.2 \text{ TeV})$ . The mono-Higgs probe considered is the SM-like Higgs state recently discovered at the large hadron collider, so as to enforce its mass reconstruction for background reduction purposes. With this in mind, its two cleanest signatures are selected:  $\gamma\gamma$  and  $ZZ^* \rightarrow 4l$  ( $l = e, \mu$ ). We show how both of these can be accessed with foreseen energy and luminosity options using a dedicated kinematic analysis performed in presence of partonic, showering, hadronisation and detector effects.

---

## Contents

<b>1</b>	<b>Introduction</b>	<b>1</b>
<b>2</b>	<b>Mono-Higgs in <math>B - L</math> SUSY models</b>	<b>3</b>
2.1	The $Z'$ sector in the BLSSM	3
2.2	The Higgs sector in the BLSSM	3
2.3	DM in the BLSSM	4
2.4	Mono-Higgs channels in SUSY models	4
2.4.1	Mono-Higgs as a final state	5
2.4.2	Mono-Higgs as an intermediate state	5
2.4.3	Mono-Higgs as an initial state	6
2.5	Analysis strategy for mono-Higgs searches in the BLSSM	6
2.5.1	LHC current exclusion and parameter space	7
2.5.2	Numerical tools	8
<b>3</b>	<b>BLSSM signals and LHC sensitivity</b>	<b>8</b>
3.1	The $\gamma\gamma + \cancel{E}_T$ signature	8
3.2	The $4l + \cancel{E}_T$ signature	11
<b>4</b>	<b>Conclusions</b>	<b>13</b>

---

## 1 Introduction

The increased pressure exercised by current experimental data on the parameter space of the Minimal Supersymmetric Standard Model (MSSM) combined with the unsatisfactory theoretical situation highlighting a severe fine-tuning problem therein (also known as the small hierarchy problem) calls for the phenomenological exploration of non-minimal constructs of Supersymmetry (SUSY) better compatible with current data than the MSSM yet similarly predictive and appealing theoretically. Because of the well established existence of non-zero neutrino masses, a well motivated path to follow in this direction is to consider the  $B - L$  Supersymmetric Standard Model (BLSSM). Herein, (heavy) right-handed neutrino superfields are introduced in order to implement a type I seesaw mechanism, which provides an elegant solution for the existence and smallness of the (light) left-handed neutrino masses. Right-handed neutrinos can naturally be implemented in the BLSSM, which is based on the gauge group  $SU(3)_C \times SU(2)_L \times U(1)_Y \times U(1)_{B-L}$ , hence the simplest generalisation of the SM gauge group (through an additional  $U(1)_{B-L}$  symmetry). In this model, it has been shown that the scale of  $B - L$  symmetry breaking is related to the SUSY breaking scale [1], so that this SUSY realisation predicts several testable signals at the Large Hadron Collider (LHC), not only in the sparticle domain but also in the  $Z'$  (a  $Z'$  boson in fact emerges from the  $U(1)_{B-L}$  breaking), Higgs (an additional singlet state is economically introduced here, breaking the  $U(1)_{B-L}$  group) and (s)neutrino sectors [2–4]. Furthermore, other than assuring its testability at the LHC, in fact, in a richer form than the MSSM (because of the additional (s)particle states), the BLSSM also alleviates the aforementioned

little hierarchy problem of the MSSM, as both the additional singlet Higgs state and right-handed (s)neutrinos [5–9] release additional parameter space from the LEP, Tevatron and LHC constraints. Finally, interesting results on the ability of the BLSSM to emulate the Higgs boson signals isolated at the LHC Run 1 have also emerged, including the possibility of explaining possible anomalies hinting at a second Higgs peak in the ATLAS and CMS data samples [10]. A Dark Matter (DM) candidate within the BLSSM which is plausibly different from the MSSM one exists as well [11].

The best probe of a DM signal at the LHC is via the mono- $j$  ( $j = \text{jet}$ ) channel for search purposes, with mono- $\gamma$ ,  $-W^\pm$  and  $-Z$  aiding most for diagnostic tasks. Herein, the keyword ‘mono’ refers to the fact that nothing but the probe appears in the detector, so that missing transverse energy is measured alongside it. In refs. [12, 13], it was pointed out that, even when the DM candidate is the same in both models<sup>1</sup>, the typical topologies of these processes can be very different between the MSSM and the BLSSM. This is due the fact that the mediator of DM pair production in the MSSM is an off-shell  $Z$  boson while in the BLSSM can naturally be a rather massive  $Z'$  boson (in the few TeV range). The peculiarity of the  $Z'$  signal decaying invisibly (directly into DM or else via heavy (s)neutrinos in turn yielding the LSPs and light neutrinos), with respect to the  $Z$  one (decaying directly into two lightest neutralinos), is that the final state mono-probe carries a very large (transverse) missing energy. Under these circumstances the efficiency in accessing the invisible final state and rejecting the Standard Model (SM) background is very high altogether compensating initially smaller production rates with respect to the  $Z$  case. Exploiting this feature, it has been shown that significant sensitivity exists already after  $300 \text{ fb}^{-1}$  during Run 2, to the extent that mono- $j$  events can be readily accessible at the LHC, so as to enable one to claim a prompt discovery, while mono- $\gamma$  as well as  $-Z$  signals can be used simultaneously as diagnostic tools of the underlying scenario.

The recent discovery of a SM Higgs boson  $h$  has however paved the way to another signal in the above category, the so-called mono- $h$  one (i.e., a mono-Higgs type) [14, 15]. The latter is not just another probe similar to the existing ones though. There is in fact a key difference between mono- $h$  and other mono-type searches. In proton-proton collisions, a  $j/\gamma/W^\pm/Z$  can be emitted directly from a light quark as Initial State Radiation (ISR) through the usual SM gauge interactions, or it may be emitted as part of the remainder of the process. In contrast, ISR induced by Higgs-strahlung is highly suppressed due to the small coupling of the Higgs boson to light quarks. Hence, unlike other mono-type signatures, a mono- $h$  signal would probe exclusively the properties of the mediator and/or DM.

It is the purpose of this paper to study the scope afforded by potential mono- $h$  signals at the LHC in the BLSSM by exploiting the fact that the  $h$  state can be emitted by massive objects, like the  $Z'$  or even an heavy Higgs boson  $h'$ , both of which can couple strongly to initial state quarks and gluons, respectively. Ideally, the mono- $h$  signal to be considered here within the BLSSM would benefit from the same kinematic features discussed above for the case of the other mono-types, thereby offering the twofold opportunity of at the same time establishing a signal of SUSY DM and characterising it as being incompatible with the MSSM. In particular, we will consider the following mono- $h$  signals:  $q\bar{q} \rightarrow Z' \rightarrow Z(\rightarrow \nu\bar{\nu})h$  and  $gg \rightarrow h' \rightarrow h(\rightarrow \tilde{\chi}_1^0 \tilde{\chi}_1^{0*})h$ , wherein the mono- $h$  probe eventually decays via  $h \rightarrow \gamma\gamma$  and  $h \rightarrow ZZ^* \rightarrow 4l$ .

The plan of our paper is as follows. The next section will be devoted to describe mono- $h$  signals arising in  $B - L$  SUSY models while the one after will present the results of our numerical analysis. In section 4, we conclude.

---

<sup>1</sup>This is typically the lightest neutralino,  $\tilde{\chi}_1^0$ , which is also the Lightest Supersymmetry Particle (LSP).

## 2 Mono-Higgs in $B - L$ SUSY models

In discussing mono- $h$  signals in the BLSSM, it is useful to recall the structure of its  $Z'$ , Higgs and DM sectors.

### 2.1 The $Z'$ sector in the BLSSM

The  $U(1)_Y$  and  $U(1)_{B-L}$  gauge kinetic mixing can be absorbed in the covariant derivative redefinition, where the gauge coupling matrix will be transformed as follows:

$$G = \begin{pmatrix} g_{YY} & g_{YB} \\ g_{BY} & g_{BB} \end{pmatrix} \implies \tilde{G} = \begin{pmatrix} g_1 & \tilde{g} \\ 0 & g_{B-L} \end{pmatrix}, \quad (2.1)$$

where

$$g_1 = \frac{g_{YY}g_{BB} - g_{YB}g_{BY}}{\sqrt{g_{BB}^2 + g_{BY}^2}}, \quad g_{B-L} = \sqrt{g_{BB}^2 + g_{BY}^2}, \quad \tilde{g} = \frac{g_{YB}g_{BB} + g_{BY}g_{YY}}{\sqrt{g_{BB}^2 + g_{BY}^2}}. \quad (2.2)$$

In this basis, one finds

$$M_Z^2 = \frac{1}{4}(g_1^2 + g_2^2)v^2, \quad M_{Z'}^2 = g_{B-L}^2 v'^2 + \frac{1}{4}\tilde{g}^2 v^2. \quad (2.3)$$

Furthermore, the mixing angle between  $Z$  and  $Z'$  is given by

$$\tan 2\theta' = \frac{2\tilde{g}\sqrt{g_1^2 + g_2^2}}{\tilde{g}^2 + 4(\frac{v'}{v})^2 g_{B-L}^2 - g_2^2 - g_1^2}. \quad (2.4)$$

### 2.2 The Higgs sector in the BLSSM

The superpotential of the BLSSM is given by

$$\hat{W} = Y_u \hat{Q} \hat{H}_2 \hat{U}^c + Y_d \hat{Q} \hat{H}_1 \hat{D}^c + Y_e \hat{L} \hat{H}_1 \hat{E}^c + Y_\nu \hat{L} \hat{H}_2 \hat{N}^c + Y_N \hat{N}^c \hat{\eta}_1 \hat{N}^c + \mu \hat{H}_1 \hat{H}_2 + \mu' \hat{\eta}_1 \hat{\eta}_2,$$

and the soft SUSY breaking terms are given by

$$\begin{aligned} -\mathcal{L}_{soft} = & m_{\tilde{q}_{ij}}^2 \tilde{q}_i^* \tilde{q}_j + m_{\tilde{u}_{ij}}^2 \tilde{u}_i^* \tilde{u}_j + m_{\tilde{d}_{ij}}^2 \tilde{d}_i^* \tilde{d}_j + m_{\tilde{l}_{ij}}^2 \tilde{l}_i^* \tilde{l}_j + m_{\tilde{e}_{ij}}^2 \tilde{e}_i^* \tilde{e}_j + m_{H_2}^2 |H_2|^2 + m_{H_1}^2 |H_1|^2 \\ & + m_{\tilde{N}_{ij}}^2 \tilde{N}_i^{c*} \tilde{N}_j^c + m_{\eta_1}^2 |\eta_1|^2 + m_{\eta_2}^2 |\eta_2|^2 + \left[ Y_{uij}^A \tilde{q}_i \tilde{u}_j H_2 + Y_{dij}^A \tilde{q}_i \tilde{d}_j H_1 + Y_{eij}^A \tilde{l}_i \tilde{e}_j H_1 \right. \\ & \left. + Y_{\nu ij}^A \tilde{L}_i \tilde{N}_j^c H_2 + Y_{Nij}^A \tilde{N}_i^c \tilde{N}_j^c \eta_1 + B\mu H_2 H_1 + B\mu' \eta_1 \eta_2 + \frac{1}{2} M_a \lambda^a \lambda^a + M_{BB'} \tilde{B} \tilde{B}' + h.c. \right], \end{aligned}$$

where  $(Y_f^A)_{ij} = (Y_f)_{ij} A_{ij}$ , the tilde denotes the scalar components of the chiral superfields as well as the fermionic components of the vector superfields and  $\lambda^a$  are fermionic components of the vector superfields. The Vacuum Expectation Values (VEVs) of the Higgs fields are given by  $\langle \text{Re} H_i^0 \rangle = v_i / \sqrt{2}$  and  $\langle \text{Re} \eta_i^0 \rangle = v'_i / \sqrt{2}$ . To obtain the masses of the physical neutral Higgs bosons, one makes the usual redefinition of the Higgs fields, i.e.,  $H_{1,2}^0 = (v_{1,2} + \sigma_{1,2} + i\phi_{1,2}) / \sqrt{2}$  and  $\eta_{1,2}^0 = (v'_{1,2} + \sigma'_{1,2} + i\phi'_{1,2}) / \sqrt{2}$ , where  $\sigma_{1,2} = \text{Re} H_{1,2}^0$ ,  $\phi_{1,2} = \text{Im} H_{1,2}^0$ ,  $\sigma'_{1,2} = \text{Re} \eta_{1,2}^0$  and  $\phi'_{1,2} = \text{Im} \eta_{1,2}^0$ . The real parts correspond to the CP-even Higgs bosons and the imaginary parts correspond to the CP-odd Higgs bosons. The mass of the BLSSM-like CP-odd Higgs  $A'$  is given by

$$m_{A'}^2 = \frac{2B\mu'}{\sin 2\beta'} \sim \mathcal{O}(1 \text{ TeV}), \quad (2.5)$$

whereas those of the BLSSM CP-even neutral Higgs fields, at tree level, are given by

$$m_{h',H'}^2 = \frac{1}{2} \left[ (m_{A'}^2 + M_{Z'}^2) \mp \sqrt{(m_{A'}^2 + M_{Z'}^2)^2 - 4m_{A'}^2 M_{Z'}^2 \cos^2 2\beta'} \right]. \quad (2.6)$$

If  $\cos^2 2\beta' \ll 1$ , one finds that the lightest  $B-L$  neutral Higgs mass is given by

$$m_{h'} \simeq \left( \frac{m_{A'}^2 M_{Z'}^2 \cos^2 2\beta'}{m_{A'}^2 + M_{Z'}^2} \right)^{\frac{1}{2}} \simeq \mathcal{O}(100 \text{ GeV}). \quad (2.7)$$

### 2.3 DM in the BLSSM

Now, we consider the neutralino sector in the BLSSM. The neutral gaugino-higgsino mass matrix can be written as [1]:

$$\mathcal{M}_7(\tilde{B}, \tilde{W}^3, \tilde{H}_1^0, \tilde{H}_2^0, \tilde{B}', \tilde{\eta}_1, \tilde{\eta}_2) \equiv \begin{pmatrix} \mathcal{M}_4 & \mathcal{O} \\ \mathcal{O}^T & \mathcal{M}_3 \end{pmatrix}, \quad (2.8)$$

where the  $\mathcal{M}_4$  is the MSSM-type neutralino mass matrix [16–19] and  $\mathcal{M}_3$  is  $3 \times 3$  additional neutralino mass matrix, which is given by

$$\mathcal{M}_3 = \begin{pmatrix} M_{B'} & -g_{B-L} v'_1 & g_{B-L} v'_2 \\ -g_{B-L} v'_1 & 0 & -\mu' \\ g_{B-L} v'_2 & -\mu' & 0 \end{pmatrix}. \quad (2.9)$$

In addition, the off-diagonal matrix  $\mathcal{O}$  is given by

$$\mathcal{O} = \begin{pmatrix} \frac{1}{2} M_{BB'} & 0 & 0 \\ 0 & 0 & 0 \\ -\frac{1}{2} \tilde{g} v_1 & 0 & 0 \\ \frac{1}{2} \tilde{g} v_2 & 0 & 0 \end{pmatrix}. \quad (2.10)$$

Note that these off-diagonal elements vanish identically if  $\tilde{g} = 0$ . In this case, one diagonalises the real matrix  $\mathcal{M}_7$  with a symmetric mixing matrix  $V$  such as

$$V \mathcal{M}_7 V^T = \text{diag}(m_{\tilde{\chi}_k^0}), \quad k = 1, \dots, 7. \quad (2.11)$$

In these conditions, the LSP has the following decomposition

$$\tilde{\chi}_1^0 = V_{11} \tilde{B} + V_{12} \tilde{W}^3 + V_{13} \tilde{H}_1^0 + V_{14} \tilde{H}_2^0 + V_{15} \tilde{B}' + V_{16} \tilde{\eta}_1 + V_{17} \tilde{\eta}_2. \quad (2.12)$$

The LSP is called pure  $\tilde{B}'$  if  $V_{15} \sim 1$  and  $V_{1i} \sim 0$  for  $i \neq 5$ , and pure  $\tilde{\eta}_{1(2)}$  if  $V_{16(7)} \sim 1$  and all the other coefficients are close to zero.

### 2.4 Mono-Higgs channels in SUSY models

In discussing mono- $h$  signals in the BLSSM, it is useful to contrast their dynamics against that of the MSSM, for which several analyses already exist [14]. In the MSSM, where the DM particle is the lightest neutralino,  $\tilde{\chi}_1^0$ , just like in our BLSSM construction, we have three classes of mono-Higgs channels, to which we will dedicate three separate subsections below<sup>2</sup>.

---

<sup>2</sup>Note that in the BLSSM versus MSSM comparison we neglect topologies where a  $h'/H'/A'$  is produced in place of the SM-like state and cascade down to it (invisibly for the rest of the event).

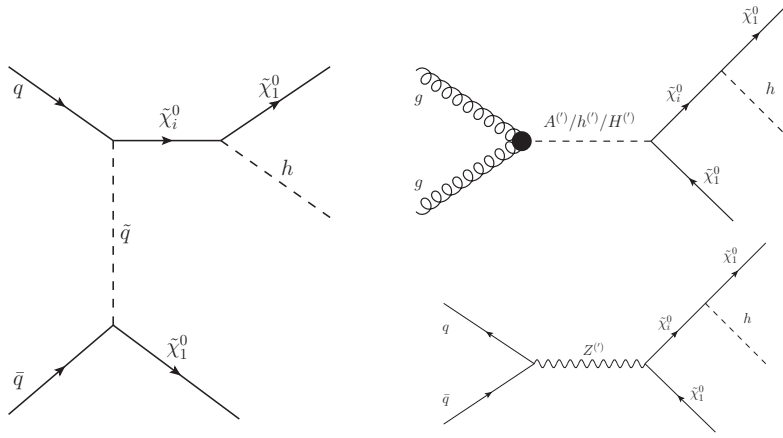


**Figure 1.** Mono-Higgs as a final state:  $q\bar{q} \rightarrow \tilde{\chi}_1^0 \tilde{\chi}_i^0 \rightarrow \tilde{\chi}_1^0 \tilde{\chi}_i^0 h$  with  $\tilde{q}$  exchange (left diagram),  $gg \rightarrow A^{(0)}/h^{(0)}/H^{(0)} \rightarrow \tilde{\chi}_1^0 \tilde{\chi}_i^0 \rightarrow \tilde{\chi}_1^0 \tilde{\chi}_i^0 h$  (top-right diagram) and  $q\bar{q} \rightarrow Z^{(0)} \rightarrow \tilde{\chi}_1^0 \tilde{\chi}_i^0 \rightarrow \tilde{\chi}_1^0 \tilde{\chi}_i^0 h$  (bottom-right diagram).

#### 2.4.1 Mono-Higgs as a final state

In this class, we have three types of MSSM channels, that we can group in two subsets depending on the mediators, see figure 1: (i)  $q\bar{q} \rightarrow \tilde{\chi}_1^0 \tilde{\chi}_i^0 \rightarrow \tilde{\chi}_1^0 \tilde{\chi}_i^0 h$  with  $\tilde{q}$  exchange, the typical value of the cross section of this channel being of order  $\mathcal{O}(10^{-7})$  pb and it is worth to note that it comes from a large  $\tilde{q}$  mass; (ii)  $gg \rightarrow A/h/H \rightarrow \tilde{\chi}_1^0 \tilde{\chi}_i^0 \rightarrow \tilde{\chi}_1^0 \tilde{\chi}_i^0 h$  and  $q\bar{q} \rightarrow Z \rightarrow \tilde{\chi}_1^0 \tilde{\chi}_i^0 \rightarrow \tilde{\chi}_1^0 \tilde{\chi}_i^0 h$ , where  $i = 2, 3, 4$ , again, the typical value of the cross section of these channels being of order  $\mathcal{O}(10^{-7})$  pb (in case of  $A$  and  $H$  mediators, these channels are suppressed due to their small production rates as well as the off-shell decay  $\tilde{\chi}_i^0 \rightarrow \tilde{\chi}_1^0 h$ , while in the case of  $h$  and  $Z$  mediators, although they have larger production rates, the suppression coming from their off-shell decays is substantial).

The BLSSM can add a few contributions to these topologies (specifically, to the two graphs on the right-hand side of figure 1). Wherever a  $Z$  is present in the MSSM, a  $Z'$  can also contribute. Furthermore, for each of the neutral MSSM Higgs states,  $h$ ,  $H$  and  $A$ , there corresponds in the BLSSM a primed version,  $h'$ ,  $H'$  and  $A'$ , wherein the  $h'$  can have a mass similar to the  $h$  one (i.e., just above 125 GeV) while the other two states are generally much heavier [10, 20–22], most notably in its inverse seesaw version [9]. Hence, the potential to increase the sensitivity of experimental analyses is twofold. On the one hand, the  $Z'$  can be produced resonantly as its current mass limits within the BLSSM enable on-shell decays  $Z' \rightarrow \tilde{\chi}_1^0 \tilde{\chi}_i^0 \rightarrow \tilde{\chi}_1^0 \tilde{\chi}_i^0 h$ , where  $i = 2, \dots, 7$ . On the other hand,  $h'$  can also be resonant in regions of parameter space where  $m_{h'} > m_h + 2m_{\tilde{\chi}_1^0}$ , which are indeed presently accessible within the BLSSM.

#### 2.4.2 Mono-Higgs as an intermediate state

In this class, we have five types of MSSM channels, that we can group in three subsets depending on the mediators, see figure 2: (i)  $q\bar{q} \rightarrow \tilde{\chi}_1^0 \tilde{\chi}_1^0 h$  with  $\tilde{q}\tilde{q}$  exchange, its typical cross section being of order  $\mathcal{O}(10^{-6})$  pb, again, this suppression stands from the large  $\tilde{q}$  mass; (ii)  $gg \rightarrow A \rightarrow Zh \rightarrow \tilde{\chi}_1^0 \tilde{\chi}_1^0 h$  (its cross section being of  $\mathcal{O}(10^{-5})$  pb due to the smallness of the production rates of the  $A$ ) and  $q\bar{q} \rightarrow Z \rightarrow Z^* h \rightarrow \tilde{\chi}_1^0 \tilde{\chi}_1^0 h$  (its cross section being very suppressed due to the off-shell decay of the

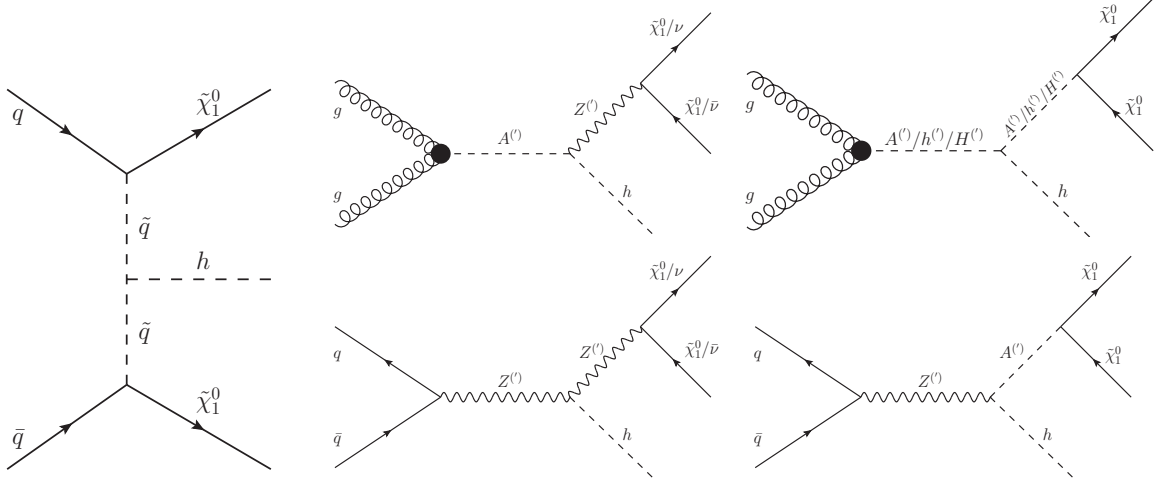


**Figure 2.** Mono-Higgs as an intermediate state:  $qq \rightarrow \tilde{\chi}_1^0 \tilde{\chi}_1^0 h$  with  $\tilde{q}\tilde{q}$  exchange (left diagram),  $gg \rightarrow A^{(\prime)} \rightarrow Z^{(\prime)} h \rightarrow \tilde{\chi}_1^0 \tilde{\chi}_1^0 h/\nu\bar{\nu}h$  plus  $q\bar{q} \rightarrow Z^{(\prime)} \rightarrow Z^{(\prime)} h \rightarrow \tilde{\chi}_1^0 \tilde{\chi}_1^0 h/\nu\bar{\nu}h$  (center diagrams) and  $gg \rightarrow A^{(\prime)}/h^{(\prime)}/H^{(\prime)} \rightarrow A^{(\prime)}/h^{(\prime)}/H^{(\prime)} h \rightarrow \tilde{\chi}_1^0 \tilde{\chi}_1^0 h$  and  $q\bar{q} \rightarrow Z^{(\prime)} \rightarrow A^{(\prime)} h \rightarrow \tilde{\chi}_1^0 \tilde{\chi}_1^0 h$  (right diagrams).

$Z$ ); (iii)  $gg \rightarrow A/h/H \rightarrow A/h/H h \rightarrow \tilde{\chi}_1^0 \tilde{\chi}_1^0 h$  (its cross section being of  $\mathcal{O}(10^{-4})$  pb owing to the dominant channel  $H \rightarrow hh$ ) and  $q\bar{q} \rightarrow Z \rightarrow Ah \rightarrow \tilde{\chi}_1^0 \tilde{\chi}_1^0 h$  (its cross section being very suppressed due to the off-shell decay of the  $Z$ ).

Within the BLSSM, again, wherever a  $Z$  is involved a  $Z'$  also is and, likewise, wherever a  $h/H/A$  enters also a  $h^{(\prime)}/H^{(\prime)}/A^{(\prime)}$  appears (this is limited to the center and right topologies in figure 2). Like previously, we expect some tangible contribution of specific BLSSM nature whenever the (heavy)  $Z'$  and/or (light)  $h'$  can resonate, so long that no heavy  $H'$  and  $A'$  states are present in the same channel.

### 2.4.3 Mono-Higgs as an initial state

In this class, we have three types of MSSM channels, each characterised by its on specific mediators, see figure 3: (i)  $q\bar{q} \rightarrow \tilde{\chi}_1^0 \tilde{\chi}_1^0 h$  with  $q\bar{q}$  exchange; (ii)  $q\bar{q} \rightarrow Zh \rightarrow \tilde{\chi}_1^0 \tilde{\chi}_1^0 h$  with  $q$  exchange; (iii)  $q\bar{q} \rightarrow A/h/H h \rightarrow \tilde{\chi}_1^0 \tilde{\chi}_1^0 h$  with  $q$  exchange. The cross sections of all these types are very suppressed due to a very small coupling of  $h$  with  $q\bar{q}$ . Moreover, in the first mode, one has the additional depletion induced by a large  $\tilde{q}$  mass.

In this case the BLSSM has little to add to the MSSM. The only possible enhancement to the overall rate could come from  $Z'$  exchange in the center diagram of figure 3 when the graph resonates, as in the left topology there is no difference while in the right one additional  $h'/H'/A'$  states are more suppressed than their un-primed versions.

## 2.5 Analysis strategy for mono-Higgs searches in the BLSSM

We initially detail the BLSSM parameter space tested, by delineating the intervals used to sample the independent parameters of this scenario assuming a low energy scale construction, then we explain in detail the numerical procedure used for this analysis, where simulated events for Signal ( $S$ ) and Background ( $B$ ) were generated through a standard sequence of a matrix element calculator, a Monte Carlo (MC) program and LHC detector software. In the two following subsections we explain how

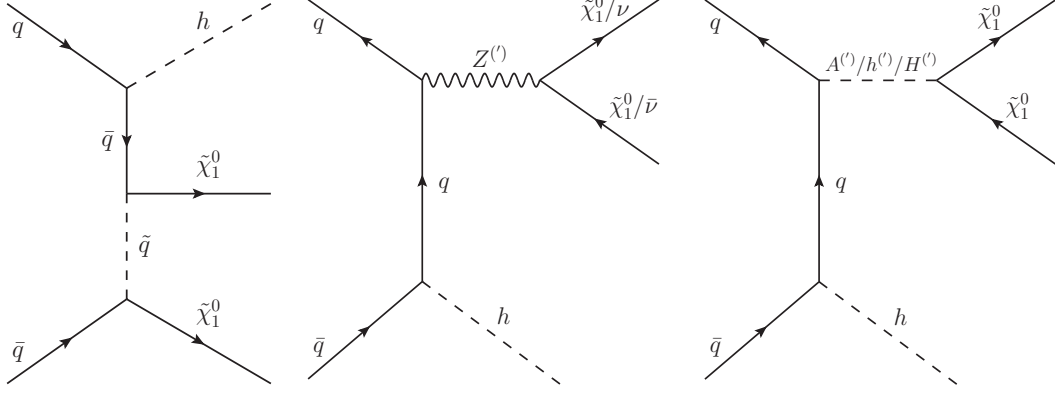


**Figure 3.** Mono-Higgs as an initial state:  $q\bar{q} \rightarrow \tilde{\chi}_1^0 \tilde{\chi}_1^0 h$  with  $q\bar{q}$  exchange (left diagram),  $q\bar{q} \rightarrow Z^{(\prime)} h \rightarrow \tilde{\chi}_1^0 \tilde{\chi}_1^0 h/\nu\bar{\nu}h$  with  $q$  exchange (center diagram) and  $q\bar{q} \rightarrow A^{(\prime)}/h^{(\prime)}/H^{(\prime)} h \rightarrow \tilde{\chi}_1^0 \tilde{\chi}_1^0 h$  with  $q$  exchange, respectively.

to extract di-photon and four-lepton signatures for our mono- $h$  probe, mediated by either  $Z'$  or  $h'$  intermediate production as, following the discussions in the previous section, these are the distinctive features of the BLSSM versus the MSSM.

### 2.5.1 LHC current exclusion and parameter space

A summary of the parameter space points used for all the signals considered here is reported in table 1. The inputs used for simulating a SM-like Higgs boson produced in association with low missing transverse energy through an  $h'$  mediator are presented in the first three rows while those for emulating a SM-like Higgs boson produced in association with high missing transverse energy mediated by a  $Z'$  are presented in the last row.

$M_{Z'}$ [GeV]	$g_{B-L}$	$\tilde{g}$	$\theta'$	$m_{h'}$ [GeV]	$m_{\tilde{\chi}_1^\pm}$ [GeV]	$m_{\tilde{g}}$ [GeV]	$m_{\tilde{\chi}_1^0}$ [GeV]
1916.5	0.27	-0.79	$1.8 \times 10^{-3}$	265.3	772	6178	10.6
1645.1	0.23	-0.89	$2.7 \times 10^{-3}$	264.7	771	6178	29.9
1468.4	0.21	-0.89	$3.4 \times 10^{-3}$	279.1	619	6185	48.6
2396.5	0.40	-0.47	$8.2 \times 10^{-4}$	332.6	920	6198	412

**Table 1.** The first three benchmark points (rows) for the  $h'$  mediated signal and the last one for the  $Z'$  mediated signal.

As intimated, we will study here the decay of heavy boson  $Z'$  and light scalar  $h'$  mediators to SM-like Higgs and some amount of missing traverse energy, where the SM-like Higgs boson decays to a  $4l$  (electrons and muons only) or  $\gamma\gamma$  final state. The presence of missing transverse energy  $\cancel{E}_T$  in the event is one of main distinguishing characteristic of the signal, which is defined as the negative sum of the transverse momenta of all reconstructed objects. Thus, it depends on the reconstruction of all charged particles, especially jets which can be responsible for inducing unwanted amounts of  $\cancel{E}_T$ . Another variable useful to reduce the background further and enhance the signal is the transverse



mass  $M_T$  of the four-lepton and di-photon systems defined as follows:

$$M_T^2(f) = \left( \sqrt{M^2(f) + p_T^2(f)} + |p_T^{\text{miss}}| \right)^2 - \left[ \vec{p}_T(f) + \vec{p}_T^{\text{miss}} \right]^2, \quad (2.13)$$

where  $M(f)$  and  $p_T(f)$  are the invariant mass and transverse momentum, respectively, of the final state particles which are  $f = \gamma\gamma$  and  $4l$ . In the end, a set of standard cuts will be chosen to enhance the  $S$ -to- $B$  ratio ( $S/B$ ), yet vetoing the above transverse mass range above 250 GeV improves the latter significantly in case of low missing transverse energy induced by the  $h'$  mediator, while this variable has less relevance for the case of a heavy mediator  $Z'$ .

It is worth to note that the spectra associated with the above mentioned benchmark points in table 1 are consistent with current LHC bounds. Also, for the  $Z'$  mass, we assured the LEP constraints:  $M_{Z'}/g_{B-L} > 6$  TeV and  $\theta' \lesssim \mathcal{O}(10^{-3})$  [23]. Moreover, the LSP satisfies the LUX bounds on the direct search for DM [24] and other direct detection experimental limits [25, 26]. However, the relic abundance depends on the details of the underlying cosmology (thermal or non-thermal abundance) so its constraints will not be considered here [27–30].

### 2.5.2 Numerical tools

Both signal and background are computed with MadGraph5 [31] that is used to estimate multi-parton amplitudes and to generate events for the calculation of the cross sections as well as for subsequent processing. The production cross sections for  $h'$  are calculated at Next-to-Leading Order (NLO) using an effective coupling calculated by SPheno [32, 33] while those for  $Z'$  mediation have LO normalisation. PYTHIA [34] is used for showering, hadronisation, heavy flavour decays and for adding the soft underlying event. The simulation of the response of the ATLAS and CMS detectors was done with the DELPHES package [35]. Reconstructed objects are simulated from the parametrised detector response and includes tracks, calorimeter deposits and high level objects such as isolated electrons, jets, taus and missing transverse momentum.

## 3 BLSSM signals and LHC sensitivity

In this section, we concentrate on mono- $h$  signals which are specific to the BLSSM, i.e., those associated to  $Z'$  and  $h'$  induced topologies, wherein these states act as mediators for DM creation. As intimated, we shall assume the SM-like Higgs state  $h$  to decay into the two channels that enable an effective Higgs mass reconstruction, so as to exploit the measured 125 GeV mass for background suppression. These are  $h \rightarrow \gamma\gamma$  and  $h \rightarrow ZZ^* \rightarrow 4l$ , where  $l = e$  or  $\mu$ . We shall do so in two separate subsections.

### 3.1 The $\gamma\gamma + \cancel{E}_T$ signature

In this subsection we study the final state with di-photons associated with missing transverse energy,  $\cancel{E}_T$ , which comes from neutrinos in the  $Z'$  mediated channel and from neutralinos in the  $h'$  mediated channel. In this analysis, we are looking for an excess over the SM predictions in the di-photon mass spectrum after a selection in terms of the missing transverse energy and/or transverse mass. For these events, pairs of photons are reconstructed to form the SM-like Higgs boson. To enhance  $S/B$  we first consider, for both  $Z'$  and  $h'$  signals, the kinematic selection used in the ATLAS analysis of ref. [36], as follows.

1. The absolute value of the pseudo-rapidity of both photon candidates is required to be below 2.5.

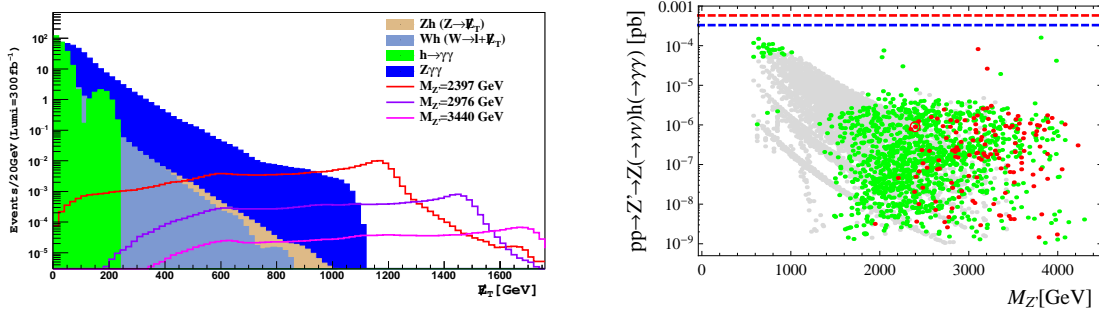


**Figure 4.** (Left panel) Number of events of both signal ( $pp \rightarrow Z' \rightarrow Zh \rightarrow \gamma\gamma + \cancel{E}_T$ ) and its relevant backgrounds generated at 14 TeV and normalised per bin width after  $300 \text{ fb}^{-1}$  of integrated luminosity versus  $\cancel{E}_T$  after considering all cuts applied by ATLAS [36]. (Right panel) The gray and green points are the signal benchmarks excluded by LEP constraints ( $M_{Z'}/g_{B-L} < 6 \text{ TeV}$  and  $\theta' > \mathcal{O}(10^{-3})$ , respectively) and the red points are the allowed ones, all mapped versus the  $Z'$  mass. The red circled point is the last benchmark point in table 1. The blue and red dashed lines are the one and two sigma exclusion limits, respectively, by ATLAS [36].

2. The invariant mass  $m_{\gamma\gamma}$  of the photon pair is required to be above 95 GeV.
3. The transverse momentum  $p_T$  of the leading (subleading) photon has to be above 30(20) GeV.
4. The  $p_T/m_{\gamma\gamma}$  ratio of the leading (subleading) photon has to be above 1/3(1/4).

Owing to the difference between the two signal mediators the set of kinematic cuts used is different depending upon whether we are looking at  $Z'$  or  $h'$  topologies. In case of a  $Z'$  mediator the most powerful observable for suppressing the background is  $\cancel{E}_T$ , which is rather large for the signal, owing to the large value of the  $Z'$  mass, see the left-hand side of figure 4. In addition, the di-photon mass spectrum characterises the signal around the  $h$  mass value, where it tends to collect owing to the underlying  $h$  resonance (this also happens for the  $Zh(\rightarrow \gamma\gamma)$ ,  $W^\pm h(\rightarrow \gamma\gamma)$  and  $h \rightarrow \gamma\gamma$  noises, though, but not for the  $Z\gamma\gamma$  continuum background). So, in the end, we enforce the following selection:  $\cancel{E}_T > 550 \text{ GeV}$  and  $110 \text{ GeV} < m_{\gamma\gamma} < 130 \text{ GeV}$ . (Notice that we also ought to veto against a high  $p_T$  and central lepton from  $W^\pm(\rightarrow l\nu)h(\rightarrow \gamma\gamma)$  events.) The benefits of this approach are clearly shown in table 2 in terms of increasing substantially  $S/B$ . However, it is obvious that the event rate associated to the chosen  $Z'$  benchmark is too poor for this becoming a viable channel at the LHC during its lifetime, including a high-luminosity option [37] (where the instantaneous luminosity of the LHC can be increased up to a factor of 10). Unfortunately, the conclusion will not change if we were to choose any other benchmark from the right-hand side of figure 4. Concerning  $h'$  topologies, owing to the much lower mediator mass involved (from  $\approx 260$  to  $\approx 280 \text{ GeV}$ ), a (necessarily low)  $\cancel{E}_T$  cut of, say, 100 GeV is not powerful to enhance  $S/B$ , in fact, both signal and background have the same  $\cancel{E}_T$  distribution, see figure 5 (left panel). However, another variable useful to reduce the background and enhance the signal is the transverse mass of the di-photon system,  $M_T(\gamma\gamma)$  of eq. (2.13), see figure 5 (right panel): by vetoing the region with  $M_T(\gamma\gamma) > 250 \text{ GeV}$  we can decrease the non-resonant background contribution significantly, as shown in table 3 (where the  $h$  mass reconstruction is enforced as well). For this topology, all three signals considered are viable at the standard LHC although kinematically they appear rather similar so that it may not be possible to distinguish one

		Backgrounds			Signal	
Process		$Z(\rightarrow \nu\bar{\nu})h$	$W(\rightarrow l\bar{\nu})h$	$h$	$Z(\rightarrow \nu\nu)\gamma\gamma$	$Z' \rightarrow Z(\rightarrow \nu\nu)h$
Before cuts		37.9	66.4	6129	9126	0.269
Cut	$n(\gamma) \geq 2$ with $p_T(\gamma) > 20$ GeV and $ \eta(\gamma)  < 2.5$	27.79	48.35	4423.6	1979.7	0.119
	$110 \text{ GeV} < m_{\gamma\gamma} < 130 \text{ GeV}$	25.81	44.65	4298.7	152.9	0.0655
	veto on $l$ with $p_T(l) > 20$ GeV and $ \eta(l)  < 2.5$	25.80	11.97	4296.1	152.8	0.0655
	$\cancel{E}_T > 550 \text{ GeV}$	0.0127	0.00059	0	0.0192	0.0459

**Table 2.** The cut flow on signal and background events for the  $\gamma\gamma + \cancel{E}_T$  signature in the  $Z'$  mediator case. These events are generated at  $\sqrt{s} = 14$  TeV with  $\mathcal{L}dt = 300 \text{ fb}^{-1}$ .

from the others. Further, as seen in figure 6, these are extracted by bulk regions of BLSSM parameter space allowed by all available experimental constraints, notably by chargino searches at the LHC, which require  $m_{\tilde{\chi}_1^\pm} > 250$  GeV by ATLAS [38] and  $m_{\tilde{\chi}_1^\pm} > 210$  GeV by CMS [39]. Hence, they are not particularly fine-tuned, rather they represent a genuine discovery scope afforded by this SUSY scenario over a substantial LSP mass range.

Before closing this section, we should dwell shortly on the backgrounds we eventually considered. Clearly, one should certainly include the irreducible background from the associated production of the  $Z$  boson and the SM-like Higgs state where the  $Z$  decays to two neutrinos, which resonates at  $m_{\gamma\gamma} \approx m_h$ . There are also two other similarly resonant backgrounds. The first one is direct SM-like Higgs production and decay, but this is reducible since it does not have real  $\cancel{E}_T$  (rather a mis-measured one from detector effects). The second one is the SM-like Higgs boson production in association with a  $W^\pm$  state where the latter decays to lepton and neutrino (wherein the lepton is missed in the detector, again leading to additional mis-measured  $\cancel{E}_T$  alongside the one emerging from the neutrino). Moreover, a continuum background which also plays a role is  $Z\gamma\gamma$ , which in fact competes with  $Zh$ . Finally, there are several non-resonant background sources that can mimic the signal when they have mis-measured  $\cancel{E}_T$  and happen to reconstruct two photons with an invariant mass close to the mass of the SM-like Higgs boson, but they were found to be negligible: these were from QCD,  $t\bar{t}$  and Drell-Yan production of two electrons.

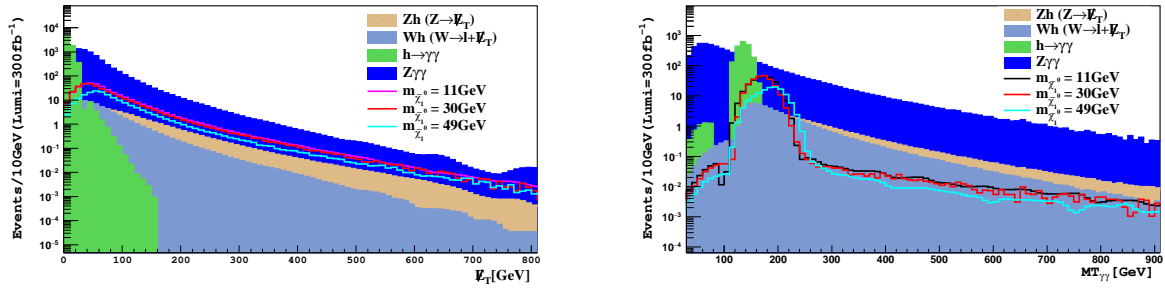


**Figure 5.** Number of events of both signal ( $pp \rightarrow h' \rightarrow hh \rightarrow \gamma\gamma + \cancel{E}_T$ ) and its relevant backgrounds generated at 14 TeV and normalised per bin width after  $300 \text{ fb}^{-1}$  of integrated luminosity versus  $\cancel{E}_T$  (left panel) and  $M_{T(\gamma\gamma)}$  (right panel) after considering all cuts applied by ATLAS [36].

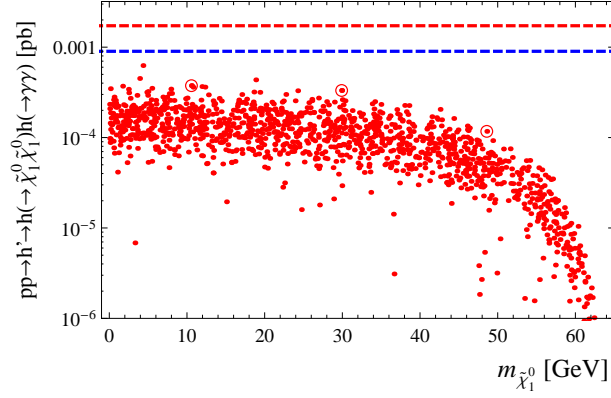


**Figure 6.** The red points are the allowed signal benchmarks mapped versus the LSP mass. The red circled points are the first three benchmark points in table 1. The blue and red dashed lines are one and two sigma exclusion limits, respectively, by ATLAS [36].

		Backgrounds				Signal		
Process		$Z(\rightarrow \nu\bar{\nu})h$	$W(\rightarrow l\bar{\nu})h$	$h$	$Z(\rightarrow \nu\nu)\gamma\gamma$	$h' \rightarrow h(\rightarrow \cancel{E}_T)h$		
Before cuts		57.0	66.3	7200	8400	386	347	183
Cut	$\cancel{E}_T > 100$ GeV	19.3	8.51	0.114	547.2	73.1	62.0	27.6
	$115 \text{ GeV} < m_{\gamma\gamma} < 130$ GeV	13.0	5.32	0.065	28.7	45.6	37.4	14.6
	$5 \text{ GeV} < M_T(\gamma\gamma) < 250$ GeV	0.88	0.51	0.030	2.01	45.4	37.3	14.5

**Table 3.** The cut flow on signal and background events for the  $\gamma\gamma + \cancel{E}_T$  signature in the  $h'$  mediator case. These events are generated at  $\sqrt{s} = 14$  TeV with  $\mathcal{L}dt = 300 \text{ fb}^{-1}$ . In the signal column, the red (left) entries are for  $m_{\tilde{\chi}_1^0} \simeq 11$  GeV, the blue (middle) entries are for  $m_{\tilde{\chi}_1^0} \simeq 30$  GeV while the green (right) entries are for  $m_{\tilde{\chi}_1^0} \simeq 49$  GeV.

### 3.2 The $4l + \cancel{E}_T$ signature

The  $h \rightarrow ZZ^* \rightarrow 4l$  decay ( $l = e, \mu$ ) has a rather small rate but it also offers a very suppressed background and for this has always been considered as the golden channel for a Higgs boson discovery. Hence, no surprise it turns out to play a significant role also in mono- $h$  searches in the BLSSM. Let us illustrate our selection strategy this time starting from the background channels one has to deal with, which are as follows.

1.  $Z(\rightarrow \nu\bar{\nu})h(\rightarrow ZZ^*)$ , which is an irreducible background.
2.  $Z(\rightarrow l\bar{l})h(\rightarrow ZZ^*)$ , which is also an irreducible background (the secondary  $Z$  is assumed to decay into neutrinos) and with a larger cross section than the previous one.
3.  $W(\rightarrow l\bar{\nu})h(\rightarrow ZZ^*)$ , where the lepton from the  $W^\pm$  (or indeed one of the others) is missed.
4.  $h(\rightarrow ZZ^*)$  with  $\cancel{E}_T$  coming from mis-measurements of soft radiation.

Other backgrounds can come from three gauge boson production: i.e.,  $Z\gamma\gamma$ ,  $WWW$ ,  $ZWW$ ,  $ZZ\gamma$ , but these are highly suppressed and can be neglected. (Also  $t\bar{t}$  production and decay is negligible here.)

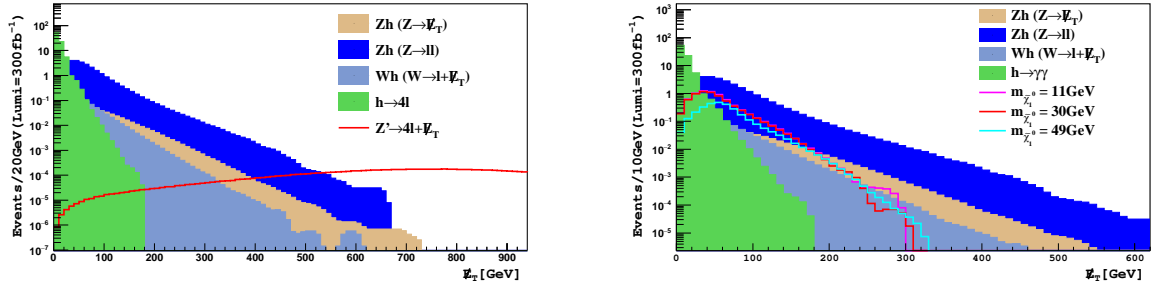


**Figure 7.** Number of events of both signals ( $pp \rightarrow Z' \rightarrow Zh \rightarrow 4l + \cancel{E}_T$  on the left plus  $pp \rightarrow h' \rightarrow hh \rightarrow 4l + \cancel{E}_T$  in the right) and their relevant backgrounds generated at 14 TeV and normalised per bin width after 300 fb<sup>-1</sup> of integrated luminosity versus  $E_T$ . The cuts described in the text have been applied here.

Events are first required to have at least four reconstructed leptons, for which we used a selection based on the CMS four lepton discovery channel of the SM-like Higgs boson. Electrons are required to have a minimum  $p_T$  of 7 GeV and need to be in the pseudorapidity range  $|\eta| < 2.5$  (which is the geometrical acceptance of both the ATLAS and CMS experiments, roughly). Selected muons need to be reconstructed with  $p_T > 6$  GeV and also be in the same geometrical acceptance. All four leptons have to be isolated. The isolation variable is defined as the sum of the transverse momenta of the tracks inside a cone of opening  $\Delta R \geq 0.3$  around the lepton. This variable is known to be robust against an increase in the number of pileup interactions and mis-identification issues. The cut on the isolation variable was optimised by using the lowest  $p_T$  lepton for each signal. Leptons of opposite sign and same flavour are then paired and any such di-lepton system is required to have an invariant mass larger than 4 GeV in order to suppress the light-jet QCD background. If more than two di-lepton pairs can be formed, ambiguities are resolved as follows: the di-lepton system with total invariant mass closest to the  $Z$  boson mass is chosen as the first  $Z$  boson. Among all valid, i.e., same flavour opposite sign, di-leptons that can be formed from the remaining tracks, we choose as the second  $Z$  boson the di-lepton system with the highest  $p_T$  whose total three-momentum vector is at least  $\Delta R \geq 0.05$  away from the first di-lepton. This set of selections is applied to both channels, i.e.,  $Z'$  and  $h'$  topologies, while the difference between the two signals can be exalted by choosing additional kinematic cuts, different from one case to the other.

The possible choice is in principle guided by figure 7, which is constructed after the above cuts are enforced on both  $Z'$  and  $h'$  topologies. In practise, though, by looking at the plot on the right-hand side, it is clear that the  $Z'$  mediator case is again irrelevant numerically, so that we will not treat it any further here. For the  $h'$  mediator case, the transverse mass variable is again highly effective to reduce the noise, thus we select events with transverse mass in range [115, 250] GeV and invariant mass of the four reconstructed leptons in the range [115, 130] GeV. At the same time we reject an event if it has missing transverse energy less than 20 GeV, as shown in table 4, wherein the  $h$  mass is also reconstructed from the four leptons). Even if less than in the case of the di-photon channel, also the four-lepton rate from mono- $h$  in the BLSSM is significant at the LHC in standard running condition, so it can be used to supplement a potential discovery herein.

Process		Backgrounds				Signal		
		$Z(\rightarrow \nu\bar{\nu})h$	$Z(\rightarrow l\bar{l})h$	$W(\rightarrow l\bar{\nu})h$	$h$	$h' \rightarrow h(\rightarrow \cancel{E}_T)h$		
Before cuts		0.654	30.0	1.11	112	7.46	7.03	2.95
Cut	$\cancel{E}_T > 20$ GeV	0.613	26.84	0.965	7.56	6.68	6.27	2.79
	$115 \text{ GeV} < m_{4l} < 130 \text{ GeV}$	0.282	0.241	0.308	0.82	1.62	1.53	0.681
	$115 \text{ GeV} < M_T(4l) < 250 \text{ GeV}$	0.177	0.207	0.199	0.82	1.62	1.53	0.681

**Table 4.** The cut flow on signal and background events for the  $4l + \cancel{E}_T$  signature in the  $h'$  mediator case. These events are generated at  $\sqrt{s} = 14$  TeV with  $\mathcal{L}dt = 300 \text{ fb}^{-1}$ . In the signal column, the red (left) entries are for  $m_{\tilde{\chi}_1^0} \simeq 11$  GeV, the blue (middle) entries are for  $m_{\tilde{\chi}_1^0} \simeq 30$  GeV while the green (right) entries are for  $m_{\tilde{\chi}_1^0} \simeq 49$  GeV.

## 4 Conclusions

We have considered the scope of current mono- $h$  searches in probing a non-minimal SUSY scenario, the BLSSM, which offers key advantages with respect to the MSSM in relation to its ability to naturally embed massive neutrinos. Rather than concentrating on mono- $h$  topologies which are common with the MSSM though, we have instead focused on those which are specific to the BLSSM. As the latter, in comparison to the former, possesses (amongst other states) an additional heavy neutral gauge boson ( $Z'$ , with mass of  $\mathcal{O}(2 \text{ TeV})$ ) as well as an intermediate Higgs ( $h'$ , with mass of  $\mathcal{O}(0.2 \text{ TeV})$ ) states, both of which may be within the LHC reach, we looked in particular at the topologies onsetting the two production and decay channels  $pp \rightarrow Z' \rightarrow Zh \rightarrow 4l + \cancel{E}_T$  and  $pp \rightarrow h' \rightarrow hh \rightarrow 4l + \cancel{E}_T$ , which indeed see a  $Z'$  and  $h'$  as mediators, respectively, of DM pair production (alongside that of neutrinos), this being the lightest neutralino. We have therefore tested the scope of the two most precise decay of the  $h$  state, into di-photons and  $Z$ -boson pairs, in extracting excesses attributable to the BLSSM above and beyond the yield of the SM. After a refined MC analysis based on multi-parton scattering, parton shower, hadronisation/fragmentation as well as detector effects, we have been able to show that a significant excess can be established by the end of the LHC Run 2 in both  $h$  decay channels in the case of the  $h'$  mediated topology, but not for the case of the  $Z'$  mediated one. A key to achieve this has been the fact that the heavier  $h'$  masses involved with respect to the one of the  $Z$  boson (the mediator of mono- $h$  events in the MSSM) afford one with rather selective criteria in improving the  $S/B$  ratio. This phenomenology occurs only for rather light LSP masses, in the range up to  $m_h/2$  (as the relevant topology proceeds via a  $h$  decay into DM pairs), yet all still allowed experimentally. Further, despite the significance of all benchmarks tested, it is not possible to extract (neither in terms of total event rates nor in terms of kinematic differences) the mass of the DM candidate. Nonetheless, our results can inform experimental searches aimed at extracting mono- $h$  signals of DM with a potential non-minimal SUSY nature in the foreseeable future, or else in imposing strong bounds on their existence.

## Acknowledgments

The work of W.A. and S.K. is partially supported by the STDF project 18448, the ICTP Grant AC-80 and the European Unions Horizon 2020 research and innovation programme under the Marie Skłodowska-Curie grant agreement No. 690575. A.H. is partially supported from the STDF project 6109 and the EENP2 FP7-PEOPLE-2012-IRSES grant. S.M. is financed in part through the NExT Institute. All authors are supported by the grant H2020-MSCA-RISE-2014 No. 645722 (NonMinimal-Higgs).

## References

- [1] S. Khalil and A. Masiero, Phys. Lett. B **665**, 374 (2008) [arXiv:0710.3525 [hep-ph]]; Z. M. Burell and N. Okada, Phys. Rev. D **85**, 055011 (2012) [arXiv:1111.1789 [hep-ph]].  
For another scenario of  $(B - L)$  symmetry breaking (through the VEV of the sneutrino), see:  
P. Fileviez Perez and S. Spinner, Phys. Rev. D **83**, 035004 (2011) [arXiv:1005.4930 [hep-ph]]; P. Fileviez Perez, S. Spinner and M. K. Trenkel, Phys. Rev. D **84**, 095028 (2011) [arXiv:1103.5504 [hep-ph]].
- [2] S. Khalil, J. Phys. G **35**, 055001 (2008) [hep-ph/0611205].
- [3] For an incomplete list, see, e.g.: L. Basso, A. Belyaev, S. Moretti and C. H. Shepherd-Themistocleous, Phys. Rev. D **80**, 055030 (2009) [arXiv:0812.4313 [hep-ph]]; L. Basso, A. Belyaev, S. Moretti, G. M. Pruna and C. H. Shepherd-Themistocleous, PoS EPS-**HEP2009**, 242 (2009) [arXiv:0909.3113 [hep-ph]]; L. Basso, S. Moretti and G. M. Pruna, Phys. Rev. D **83**, 055014 (2011) [arXiv:1011.2612 [hep-ph]]; L. Basso, A. Belyaev, S. Moretti and G. M. Pruna, J. Phys. Conf. Ser. **259**, 012062 (2010) [arXiv:1009.6095 [hep-ph]]; S. K. Majee and N. Sahu, Phys. Rev. D **82**, 053007 (2010) [arXiv:1004.0841 [hep-ph]]; T. Li and W. Chao, Nucl. Phys. B **843**, 396 (2011) [arXiv:1004.0296 [hep-ph]]; P. Fileviez Perez, T. Han and T. Li, Phys. Rev. D **80**, 073015 (2009) [arXiv:0907.4186 [hep-ph]]; W. Emam and S. Khalil, Eur. Phys. J. C **55**, 625 (2007) [arXiv:0704.1395 [hep-ph]].
- [4] S. Khalil and S. Moretti, J. Mod. Phys. **4**, 7 (2013) [arXiv:1207.1590 [hep-ph]] and Front. Phys. **1**, 10 (2013) [arXiv:1301.0144 [physics.pop-ph]].
- [5] A. Elsayed, S. Khalil and S. Moretti, Phys. Lett. B **715**, 208 (2012) [arXiv:1106.2130 [hep-ph]]; L. Basso and F. Staub, Phys. Rev. D **87**, 015011 (2013) [arXiv:1210.7946 [hep-ph]].
- [6] B. O’Leary, W. Porod and F. Staub, JHEP **1205**, 042 (2012) [arXiv:1112.4600 [hep-ph]]; S. Khalil and H. Okada, Phys. Rev. D **79**, 083510 (2009) [arXiv:0810.4573 [hep-ph]].
- [7] L. Basso et al., Comput. Phys. Commun. **184**, 698 (2013) [arXiv:1206.4563 [hep-ph]]; G. Brooijmans et al., arXiv:1203.1488 [hep-ph].
- [8] A. Elsayed, S. Khalil, S. Moretti and A. Moursy, Phys. Rev. D **87**, 053010 (2013) [arXiv:1211.0644 [hep-ph]].
- [9] S. Khalil and S. Moretti, arXiv:1503.08162 [hep-ph].
- [10] W. Abdallah, S. Khalil and S. Moretti, Phys. Rev. D **91**, 014001 (2015) [arXiv:1409.7837 [hep-ph]].
- [11] L. Basso, B. O’Leary, W. Porod and F. Staub, JHEP **1209**, 054 (2012) [arXiv:1207.0507 [hep-ph]]; S. Khalil and H. Okada, Phys. Rev. D **79**, 083510 (2009) [arXiv:0810.4573 [hep-ph]].
- [12] W. Abdallah, J. Fiaschi, S. Khalil and S. Moretti, Phys. Rev. D **92**, 055029 (2015) [arXiv:1504.01761 [hep-ph]].
- [13] W. Abdallah, J. Fiaschi, S. Khalil and S. Moretti, JHEP **1602**, 157 (2016) [arXiv:1510.06475 [hep-ph]].
- [14] L. Carpenter, A. DiFranzo, M. Mulhearn, C. Shimmin, S. Tulin and D. Whiteson, Phys. Rev. D **89**, 075017 (2014) [arXiv:1312.2592 [hep-ph]]; A. Berlin, T. Lin and L. T. Wang, JHEP **1406**, 078 (2014) [arXiv:1402.7074 [hep-ph]]; J. M. No, Phys. Rev. D **93**, 031701 (2016) [arXiv:1509.01110 [hep-ph]]; A. A. Petrov and W. Shepherd, Phys. Lett. B **730**, 178 (2014) [arXiv:1311.1511 [hep-ph]].
- [15] A. Nelson, <http://cds.cern.ch/record/1754504/files/ATL-PHYS-SLIDE-2014-625.pdf>.
- [16] H. E. Haber and G. L. Kane, Phys. Rept. **117**, 75 (1985).
- [17] J. F. Gunion and H. E. Haber, Nucl. Phys. B **272**, 1 (1986) [Erratum-ibid. B **402**, 567 (1993)].
- [18] M. M. El Kheishen, A. A. Aboshousha and A. A. Shafik, Phys. Rev. D **45**, 4345 (1992).

- [19] M. Guchait, Z. Phys. C **57**, 157 (1993) [Erratum-ibid. C **61**, 178 (1994)].
- [20] A. Hammad, S. Khalil and S. Moretti, Phys. Rev. D **92**, 095008 (2015) [arXiv:1503.05408 [hep-ph]].
- [21] S. Khalil and S. Moretti, arXiv:1510.05934 [hep-ex].
- [22] A. Hammad, S. Khalil and S. Moretti, Phys. Rev. D **93**, 115035 (2016) [arXiv:1601.07934 [hep-ph]].
- [23] G. Cacciapaglia, C. Csaki, G. Marandella and A. Strumia, Phys. Rev. D **74**, 033011 (2006) [hep-ph/0604111]; M. Carena, A. Daleo, B. A. Dobrescu and T. M. P. Tait, Phys. Rev. D **70**, 093009 (2004) [hep-ph/0408098].
- [24] D. S. Akerib et al. [LUX Collaboration], Phys. Rev. Lett. **116**, 161301 (2016) [arXiv:1512.03506 [astro-ph.CO]].
- [25] E. Aprile [XENON1T Collaboration], Springer Proc. Phys. **148**, 93 (2013) [arXiv:1206.6288 [astro-ph.IM]].
- [26] E. Aprile et al. [XENON100 Collaboration], Phys. Rev. Lett. **109**, 181301 (2012) [arXiv:1207.5988 [astro-ph.CO]].
- [27] E. W. Kolb and M. S. Turner, The Early Universe, Redwood City, USA: Addison-Wesley (1988) 719 pp., (Frontier in Physics, 70).
- [28] G. F. Giudice, E. W. Kolb and A. Riotto, Phys. Rev. D **64**, 023508 (2001) [hep-ph/0005123].
- [29] T. Moroi and L. Randall, Nucl. Phys. B **570**, 455 (2000) [hep-ph/9906527].
- [30] W. Abdallah and S. Khalil, Adv. High Energy Phys. **2016**, 5687463 (2016) [arXiv:1509.07031 [hep-ph]].
- [31] J. Alwall et al., JHEP **1407**, 079 (2014) [arXiv:1405.0301 [hep-ph]].
- [32] W. Porod, Comput. Phys. Commun. **153**, 275 (2003) [arXiv:hep-ph/0301101].
- [33] W. Porod and F. Staub, Comput. Phys. Commun. **183**, 2458 (2012) [arXiv:1104.1573 [hep-ph]].
- [34] T. Sjostrand, S. Mrenna and P. Z. Skands, JHEP **0605**, 026 (2006) [hep-ph/0603175].
- [35] J. de Favereau et al. [DELPHES 3 Collaboration], JHEP **1402**, 057 (2014) [arXiv:1307.6346 [hep-ex]].
- [36] G. Aad et al. [ATLAS Collaboration], Phys. Rev. Lett. **115**, 131801 (2015) [arXiv:1506.01081 [hep-ex]].
- [37] F. Gianotti et al., Eur. Phys. J. C **39**, 293 (2005) [hep-ph/0204087].
- [38] G. Aad et al. [ATLAS Collaboration], Eur. Phys. J. C **75**, 208 (2015) [arXiv:1501.07110 [hep-ex]].
- [39] V. Khachatryan et al. [CMS Collaboration], Phys. Rev. D **90**, 092007 (2014) [arXiv:1409.3168 [hep-ex]].